A Satellite Infrared Technique for Diurnal Rainfall Variability Studies

Emmanouil N. Anagnostou
Universities Space Research Association
Laboratory for Atmospheres
NASA/Goddard Space Flight Center
Greenbelt, MD 20771

Andrew J. Negri and Robert F. Adler
Laboratory for Atmospheres
NASA/Goddard Space Flight Center
Greenbelt, MD 20771

Submitted to: *Journal of Geophysical Research-Atmospheres*
Corresponding author: Emmanouil N. Anagnostou
November 1998

1. Introduction

Reliable information on the distribution of precipitation at high temporal resolution (<1 hour) is essential for understanding the characteristics of convection in a region. Cloud-top infrared (IR) brightness temperatures from geostationary platforms have a weak physical connection to precipitation, however, their high sampling frequency makes them attractive in studying the temporal evolution of cloudiness and convection. On the other hand, microwave-based observations from lower sampling-frequency polar-orbiting platforms can provide a better physical connection to precipitating hydrometeors. A recent invention in rainfall estimation from a combination of these two sensors involves adjustment of IR estimates using co-existing MW-based precipitation data on a monthly basis (Adler et al., 1994; Huffman et al., 1995). These techniques use the MW data to remove systematic errors in IR rain estimates, while retaining the high sampling frequency of IR observations (approximately every 15-30 minutes).

Perhaps of even greater importance to climate and hydrometeorological applications is the separation of mesoscale convective systems into a portion of rain associated with deep convection (hereafter called convective precipitation), and to precipitation falling from more

widespread anvil clouds (hereafter called stratiform precipitation). Convective precipitation is concentrated within regions of the cumulonimbus with unstable vertical moist static energy distribution, where hydrometeors rapidly increase their mass by collecting cloud water and precipitating in heavy showers (Houze, 1993). Stratiform precipitation falls in regions of older convection where the vertical air motion is generally weaker. Although the rainrates from stratiform systems are much weaker than from the adjacent convective cells, the stratiform precipitation covers larger areas and contributes to a significant portion (40%-50%) of the rainfall volume of major convective systems. The two precipitation regions of tropical convective systems have distinctly different thermodynamic structures, hence different latent heating profiles. For example, at low altitudes young convective cells heat the atmosphere due to condensation of water vapor, while in regions of older convection evaporation of raindrops drifting downward cool the atmosphere (Houze, 1997; Tao et al., 1993a,b). This difference in heating profiles has implications in global climate (Hartmann et al., 1984). Therefore, proper validation of rain and heating patterns predicted by global circulation models (Cess et al., 1993) would require separate evaluation of the convective rain component from the remaining precipitation.

Satellite-based precipitation classification schemes have been developed for MW-only (e.g., Anagnostou and Kummerow, 1997; Kummerow et al., 1996; Greenwald et al., 1993), IR-only (Adler and Negri, 1988), and combined MW-IR (e.g., Liu et al., 1995) data. The schemes which involve MW data, though more accurate in estimating surface rainfall rates, are not quite as useful in studying the evolution of the convective and stratiform components of the mesoscale systems. A recent study by Short et al. (1997) based on shipboard radar data demonstrated that convective and stratiform precipitation over tropical oceans has significant diurnal variation. Apart from limited field experiments, the coverage of surface rainfall measuring networks over tropical land (e.g., rainforests) and ocean is sparse. Studying the mesoscale dynamics of convective systems in these regions is feasible only from geosynchronous satellites (e.g. Garstang et al., 1994; Garreaud and Wallace, 1997).

This current research, expanding on the work of Adler and Negri (1988), focuses on estimation of tropical convective and stratiform rainfall. We attempt to answer fundamental questions, such as: is estimation of convective and stratiform precipitation from IR feasible? If so, how accurate can this be? What is the scale dependence of the IR algorithm's performance? To address these questions, quantitative comparisons are performed between coincident IR- and MW-based

instantaneous rainfall estimates at the MW 85 Ghz resolution (~12.5 km).

Our data set spans a three-month period (January to March, 1996) of MW and IR observations over northern South America (15N-15S and 35W-80W), which includes the Amazon river basin. We classify precipitation estimates with respect to the time of the satellite overpass. In the period of this study there were two polar-orbiting satellites (F10 and F11/13) with the Special Sensor Microwave/Imager (SSM/I) aboard, providing a maximum of four MW observations per day at 06, 10, 18, and 22 local time (LT). The NASA Goddard PROFiling (GPROF) algorithm is used to retrieve rainfall from the SSM/I observations (Kummerow et al., 1996). The convective and stratiform separation on the MW rain retrievals is performed based on the Anagnostou and Kummerow (1997) technique. The histograms of convective and stratiform GPROF rain rate estimates for the study period are shown in Figure 1. Convective precipitation covers less than a quarter of the total rain area, but it accounts for almost half of the rain volume. The mean convective rain rate is 10.8 mm/h; the mean stratiform rain rate is 4.1 mm/h.

The IR technique described herein considers convective rain as being associated with the presence of local minima of the IR cloudiness (T<253K). We define a variable (T_{mode}), which is the most frequently occurring temperature of a cloud system

with 253K boundary temperature (Adler et al., 1985). The total rain area within the 253K cloudiness is inversely related to T_{mode}, and directly related to the cloud area within the T_{mode} boundary. This is similar to the Adler and Negri (1987) aproach where T_{mode} was sought as an indicator of the anvil background temperature. The convective rain area is directly related to a convective index (CI), which represents the volume of convective cores exceeding the cloud system's anvil background (at near-tropopause). Rain rate is assigned to the convective and stratiform areas based on IR temperature-MW rainrate probability matching lookup tables.

In this paper we present the development and testing of the technique, and its application to study the diurnal cycle of convection over the Amazon basin and surrounding areas. Detailed description of the technique's components is provided in section 2. In section 3 we test the performance of the technique. Results from implementing the technique over the northern South America region are presented in section 4. We summarize in section 5.

2. Description of the technique

The proposed technique is designed to produce instantaneous convective and stratiform rain rate maps based on brightness temperature measurements from the Geostationary

Abstract

The development of a satellite infrared technique for estimating convective and stratiform rainfall area and volume, and its application in studying the diurnal variability of rainfall in Amazonia are presented. Cloud systems are defined in the technique by the 253K infrared (IR) temperature isotherm. The convective and stratiform rain areas within these cloud systems are then related to morphologic characteristics of the IR temperature fields. Rainfall rates are assigned to the defined convective and stratiform areas using IR-microwave-derived rainrate probability matching relationships. The training data set consists of three months of collocated IR observations and microwave (MW) rainrate retrievals over a region in the Amazon basin. Evaluation of instantaneous rain rate estimates over a second independent region in the Amazon showed 25%(-40%) systematic error, and 55%(70%) residual random error standard deviation, in morning (evening) MW overpasses. The method is used to derive the mean diurnal cycle of rainfall, and investigate the relative contribution from its convective and stratiform components. Finally, the technique is applied to study the time evolution of rainfall and the transition from convective to stratiform over selected sites in the Amazon.

Operational Environmental Satellite (GOES) infrared (10.5-12.6 μm) channel. The goal is to derive convective and stratiform rain area and rate distributions which resemble the features seen in MW rainfall estimates. The resolution of the retrieved rainfall maps is of the field of view of the 85Ghz MW sensor (12.5 km by 12.5 km). The technique is formulated in a general way, which should allow its transportability to various rain regimes.

The technique's parameters are estimated based on three months (January to March, 1996) of collocated IR temperatures and MW rain estimates. The area of study is the Amazon basin and the northeast coast of South America. For testing the technique's performance we selected two equal size regions within the study area, which where used for calibration and validation. Figure 2 shows the study area and the calibration-validation regions. Collocated GOES-8 IR temperatures, and rainrates derived from GPROF algorithm (Kummerow et al., 1996) applied on the SSM/I MW data, are used. Both data are grided at 12.5km (0.108°) resolution. Table 1 shows the calibration and validation data sample statistics. The technique's components are described next.

a. Assignment of the rain areas

The technique first determines the convective and stratiform precipitation regions within a cloud system. This is a multiple step process. The cloud systems are defined by delineating clusters of 253K temperatures within the IR brightness temperature (BT) array. A histogram of IR values yields the most frequently occuring IR temperature (T_{mode}) for each cloud system. The area of IR temperature less than T_{mode} is linearly related to the total MW-estimated rain area within the cloud system. Figure 3 shows scatter plots of T_{mode} area (A_{mode}) versus the MW total rain area (A_{tot}) for the cloud systems within the calibration area. The scatter plots are presented for six T_{mode} classes: <210K, 210-220K, 220-230K, 230-240K, 240-250K, >250K. Based on the above figure we define the following relationship for the total rain area within a cloud system:

$$A_{tot} = f_T \, A_{mode} \qquad (1)$$

The slopes, f_T, of the relationship for the different T_{mode} classes are reported in Table 2. For cloud systems with cold T_{mode} values (<220K), the largest portion of the T_{mode} area is assigned to rain. This is similar to the Adler and Negri (1988) approach, which assigns rain to the IR pixels with values lower than T_{mode}; the typical T_{mode} values in that study

were colder than 220K. For cloud systems with warm (> 240K) T_{mode} values the area assigned to rain are less than 18% of the T_{mode} area. These systems represent warm, low elevation clouds, with little precipitation.

The next step is to determine the convective regions within the rain area assigned to each cloud system. The stratiform area would then be the remainder rain area. The convective rain area estimation is based on the following steps. First, the GOES-8 IR temperature array is searched for local minima, designated T_{min}. Following Adler and Negri (1988), if the minima encompass more than one IR pixel, the location of their centroid is used. The summation of the differences between the T_{min} values and the cloud's T_{mode} value is one measure of the intensity of convection within the cloud system. The scatter plots of Figure 4 demonstrate this point. In this figure the MW-derived convective rain areas of each cloud system in the calibration site are plotted against a parameter we call the convective index (CI):

$$CI = \frac{1}{T_{mod\,e}} \sum_{i=1}^{N} \left(T_{mod\,e} - T_{min}^{i} \mid T_{min}^{i} < T_{mod\,e} \right) \qquad (2)$$

where N is the number of IR minima within a cloud system. The CI variable physically represents the magnitude of convective cloudiness within a cloud system which is above the T_{mode}

threshold. For deep convective systems T_{mode} is close to the equilibrium level or tropopause temperature (Adler and Negri, 1988). We define a linear relationship between CI and the convective rain area, A_{CNV}, within a cloud system:

$$A_{CNV} = \max\{(A_{C0} + f_C \, CI), \, 0\} \qquad (3)$$

where A_{C0} and f_C are the linear relationship's coefficients, whose values, reported in Table 2, depend on the cloud system's T_{mode}. The steps involved in the convective-stratiform (C/S) rain area estimation procedure are summarized as:

- Delineate the 253K cloud systems in the IR array;
- Evaluate the T_{mode} value and A_{mode} area for each system;
- Identify the local minima in the IR array, and calculate the CI for each system;
- Evaluate each system's total rain area from Equation (1);
- Evaluate the convective portion of each cloud system's rain area from equation (3);
- Define the remaining rain area as stratiform;
- Apply convective and stratiform rain area to coldest IR temperatures, applying the convective area first.

A schematic demonstration of the convective-stratiform area delineation procedure is provided in Figure 5. In the upper panels we show four typical examples of IR cloudiness with its associated T_{mode} temperature boundaries (blue contours), and identified local minima (T_{min}) locations (red crosses). The middle panels show the C/S rain areas determined from the above parameters, while the lower panels show the corresponding MW derived C/S rain areas. The time differences between corresponding MW and IR observations are within 15 minutes. The convective and stratiform areas are designated with red and blue, respectively. Careful inspection of this figure shows that the IR algorithm can retrieve even some of the small scale convective and stratiform features seen in the MW data.

b. Assignment of rain rates

After the C/S rain areas have been identified, the final step is to assign rainrates within these areas. This step requires a relationship between IR temperatures and rain rates. The conversion relationships are different for the convective and stratiform precipitation regions. The relationships are derived in a probabilistic way. We developed look-up tables of IR temperature depresion (T_{dif}=253-T) and microwave-rainrate pairs with the same cumulative

probability. We defined separate T_{dif}-rainrate relationships for convective and stratiform, and four T_{mode} classes: <210K, 210-220K, 220-230K, >230K. These relationships, which are plotted in Figure 6, are used to convert IR temperatures of the selected convective and stratiform areas to rainrates. Like the CST (Adler and Negri, 1988) the convective rainrates range from about 2 to 25 mm/h; while the stratiform rainrate in the CST was fixed at 2 mm/h, here it is allowed to vary between 0 and 10 mm/h.

3. Evaluation of the technique

In this section we evaluate the ability of the technique to estimate the convective and stratiform rain areas and rain volumes at the spatial scales associated with the cloud system definition. The region used for validation is shown in Figure 2. This region has the same size (15° by 10°) as the calibration region. The reference data source is instantaneous C/S rain estimates from MW observations. We first present typical examples of instantaneous IR-estimated and GPROF-retrieved rainrate maps (see Figure 7). Visual inspection of Figure 7 shows that the zero-rain intermitency in the instantaneous IR rainrate fields agrees with the zero-rain intermitency in the MW data. However, MW rain fields have higher conditional (nonzero rain) spatial rainfall

variability than IR rain fields. It should be also noted, that part of the differences seen in the MW-IR comparisons are due to the temporal mismatches (up to 15 minutes) of the two sensors.

In Figure 8 we show scatter plots of instantaneous cloud system C/S rain areas and rain volumes (Figure 9) derived from corresponding IR and MW observations. The IR-MW pairs are classified into four panels which correspond to the four times of SSM/I overpasses per day: 06, 10, 18, and 22 LT. Comparison of Figures 8 and 9 shows that GPROF-IR rain-area differences can explain most of the differences in the rain-volumes, which is due to the high correlation between rain area and rain volume for large systems (Atlas et al., 1990). The corresponding MW(GPROF)-IR conditional rain volume and area difference statistics are presented in Table 3. The conditioning is that at least one of the GPROF or IR pair values is non-zero. The statistics are the correlation coefficient (CC), the fractional standard error (FSE), and the normalized bias (NBIAS), obtained as following:

$$CC = \left(\frac{\frac{1}{N}\sum_{i=1}^{N}\left(R_i^G R_i^I\right) - \frac{1}{N^2}\sum_{i=1}^{N} R_i^G \sum_{i=1}^{N} R_i^I}{\frac{1}{N}\sqrt{\sum_{i=1}^{N}\left(R_i^G - \overline{R}^G\right)\sum_{i=1}^{N}\left(R_i^I - \overline{R}^I\right)}} \right)^{0.5} \qquad (4)$$

$$FSE = 100\left(\frac{\frac{1}{N}\sum_{i=1}^{N}\left(R_i^G - R_i^I\right)^2}{\frac{1}{N}\sum_{i=1}^{N}\left(R_i^G - \bar{R}^G\right)^2}\right)^{0.5} \quad (5)$$

$$NBIAS = 100\,\frac{\frac{1}{N}\sum_{i=1}^{N}\left(R_i^G - R_i^I\right)}{\frac{1}{N}\sum_{i=1}^{N}R_i^G} \quad (6)$$

where N is the number of cloud systems in the validation site, and R^G and R^I represent MW(GPROF) and IR rain volume (mm km^2) or area (km^2), respectively. The technique underestimates (overestimates) morning (evening) convective and stratiform rainfall area and volume. The morning bias is about 40%, while the evening bias is approximately 25%. The normalized standard deviation of the MW(GPROF)-IR instantaneous rain volume, and area, differences is 70% for the morning samples, and 55% for the evening samples.

We now evaluate the technique at four 2° by 2° grid areas in the Amazon basin (see Figure 2). Three of these areas are outside the region used for calibration. The selection of the locations was made according to the regional climatology, which shows that they receive large rainfall amounts and have one of the highest morning-evening rainfall differences in the region (Negri et al., 1996). The reference rainfall data

source is instantaneous 2°-average convective and stratiform MW rainfall averages. Figure 10 shows the MW(GPROF) and IR estimated convective and stratiform mean (January-March) rainfall for the four times of the day that MW observations are available. Overall, the IR technique predicts well the mean diurnal variation of convective and stratiform rainfall derived from MW data. Near the coast, though, (site 3) where sea breeze is the main source of evening convection, the IR technique results in an overestimation of the total convective and stratiform rain in the evening. The technique's mean diurnal predictions at site 4 have the least bias, but this was expected as this site is located within the calibration region.

The MW(GPROF)-IR area-rainfall difference statistics (CC, FSE, NBIAS) for the four selected sites are shown in Table 4. Statistics are not evaluated for sites 3 and 4 at the 06LT and 10LT times because of the small conditional sample size (<10). The typical sample size is about 20 conditional rain pairs. Overall, we see high correlation between MW(GPROF) and IR instantaneous area-averaged rainfall rates. The technique underestimates the morning rain volume, while it predicts more rain during the evening. For sites 3 and 4 the high morning relative bias should not be of great concern, since precipitation during these morning hours is negligible with respect to the total daily rain volume. Although, there is

still some diurnal bias aparent in the IR technique's estimates, the improvement from using a single IR-MW rainrate relationship (e.g., Arkin and Meisner, 1987) has been significant. To demonstrate this, we evaluated a single IR-rainrate relationship based on the calibration site's MW-IR database. The relationship uses a look-up table, which shows the corresponding MW-rainrate and IR-temperature values with equal area coverages. The relationship is shown in Figure 11. Table 5 shows for the single relationship method the same MW-IR rainrate difference statistics presented in Table 4. One can observe that although the correlations of the two methods are similar, the single threshold method has significantly higher diurnal biases than the technique presented herein. For example, at site 1 the single threshold 18LT-06LT bias difference is 67.5%, while for the new technique this difference is 42.6% (37% reduction). Another important point is the reduction of the normalized variance of the MW-IR rainrate differences. This variance reduction ranges from 35% to 40%, and between 20% and 65%, for the morning and evening overpasses, respectively.

4. Application of the technique

We apply the MW-calibrated IR convective-stratiform technique to evaluate the diurnal variability of convection in

the Northern South America region for a time period of four months (Jan-Apr). The issues examined include: (1) the diurnal variability of the 0.5° monthly precipitation; (2) the probability distributions of convective and stratiform rainfall; and (3) the diurnal variability of the convective and stratiform components of monthly precipitation at selected 2° by 2° grids.

Figure 12 shows the mean diurnal cycle for the total convective and stratiform rainfall at half degree resolution. The panels reading from left to right and top to bottom correspond to hourly time ranges: 0-1, 1-2, [...], 22-23, 23-24 GMT. Convection initiates at around 16 local time and continues throughout the night. Most of the evening convection occurs (1) along the northeast coast (on-shore-side), (2) over the area where Negro and Solimo rivers merge to form the Amazon river, and (3) along the rivers of Mato Grosso plateau. The convection seems to have an east-west propagation. Early in the morning (02-06 LT) we see convection enhancement (1) over the western part of the Amazon river, (2) along the eastern slopes of the Andes, (3) along the east coast (on-ocean-side) near the mouth of the Amazon river, and (4) at the gulf of Panama. One can also notice a significant river effect on convection, which is primarily a day time phenomenon (see for example the stretch of the Amazon river between 60W and 52W).

The IR technique also allowed us to evaluate the histograms of convective and stratiform rainfall rates at 12.5 km resolution. The histograms are shown in Figure 13. Overall, convective precipitation in the IR retrievals covers 21% of the total rain area, and contributes about 46% of the rain volume. These results are controlled by the MW convective and stratiform rain characteristics (see Figure 1), which were used for calibration of the technique. Therefore, the validity of these values depends on the accuracy of the MW C/S rain retrievals over land.

Figure 14 shows the mean diurnal cycle of the convective and stratiform components of precipitation for the four 2° by 2° sites shown in Figure 2. We can see distinct differences in the diurnal rainfall variations between the four sites. Site 3, which represents coastal convection, seems to have the highest morning versus evening difference. Site 2, which is in the convergence region of the Negro and Orinoco rivers, shows much lower rainfall variations throughout the day. It seems that the inland sites have much higher morning to early afternoon convection than the sites closer to the coast, where most of the convection is over the ocean. Figure 14 also shows an approximate 1-1.5 hours time-lag between convective and stratiform area-rainfall peaks. Mean stratiform rainfall is higher than convective rainfall during the late evening and early morning hours. This difference is more apparent for the

sites closer to the coast. Analyzing all four months of IR C/S rain retrievals indicated that rainfall in the Amazon region, initiated by land-ocean circulation and topographically driven convective processes, transitions from convective to stratiform while it propagates from east to west. The convective versus total rainfall volume ratios for the four sites are .49, .47, .48, and .51, respectively.

Examples of typical time series of convective and stratiform area-averaged rainfall over the four sites are shown in Figure 15. Viewing time series of C/S rainmaps indicated frequent sequences of convective rainfall with trailing regions of stratiform rain. Area-averaged convective rainfall based on these retrievals has a life cycle of up to 8 hours, while stratiform rain lasts much longer (>15 hrs). The IR-derived area-averaged convective-stratiform sequences seen in the 2° grids are qualitatively similar to observations by radar at other tropical sites (see for example Figure 11 in Short et al., 1997). Although, this fact should not be interpreted as proof of validity of the rainfall estimation algorithm, it suggests that the technique may be valid in observing the diurnal variability of convective and stratiform rainfall. Studies of this kind, which utilize the technique discussed herein along with over a year of IR data from the Amazon region, are under way and will be reported in separate publications.

5. Conclusions and future work

A method for estimating convective and stratiform precipitation areas and area-averaged rainrates has been described. The method which builds upon the Adler and Negri (1988) Convective-Stratiform Technique (CST) has the following characteristics. It works in the context of cloud systems, which are clusters of 253K isotherms identified within the IR brightness temperature array. Due to the well recognized difficulty of connecting IR temperatures to rainfall rates at the pixel resolution, the technique utilizes predictors which represent average morphologic characteristics of the identified cloud systems. These predictors are: the area covered by IR temperatures less than the most frequent temperature (T_{mode}) of a cloud system, and the sum of only positive differences between T_{mode} and the cloud system's local temperature minima (equation 2). Linear regressions have been applied to relate the above predictors to the cloud systems' convective and total rain areas. Rainfall rate is assigned to the identified convective and stratiform areas based on temperature-rainrate lookup tables derived using the probability matching approach.

The technique was calibrated and evaluated using MW rain estimates, derived from the GPROF (Kummerow et al., 1996)

algorithm, as a reference data source. The calibration and validation database came from collocated IR-MW observations over two 15° by 10° regions in the Amazon basin for a period of three months (January-March, 1996). The technique was evaluated with respect to its ability to predict convective and stratiform rain areas and volumes at spatial scales of the size of the identified cloud systems. These scales ranged from a few hundreds up to several thousands of square kilometers. We showed good correlation between MW(GPROF) and IR convective and stratiform rain areas and volumes. Overall, the technique's total rain volume predictions had a bias of about -40% and 25% in the morning and evening MW-IR comparisons, respectively. The higher morning bias is not of great concern, though, due to the low precipitation at these hours of the day. The technique's normalized standard deviation of the instantaneous rainfall estimation error in the morning and evening hours is 70% and 55%, respectively. Results of this study are being evaluated to hopefully improve the technique to eliminate the remaining bias errors in the estimation of the diurnal cycle.

The technique's ability to predict the mean diurnal variation of the convective and stratiform component of precipitation at 2° grids was evaluated against MW observations available at four times of the day (06, 10, 18, and 22 LT). It is worth noting that the IR estimates could successfully

depict the spatial variability in the mean diurnal cycle of the MW rain retrievals.

The technique was subsequently applied to four months (January-April, 1996) of IR-only data over the Northern South America to study the diurnal cycle of convective and stratiform rainfall. Climatological maps of the mean rainfall rate at 2-hourly intervals were presented at 0.5° spatial resolution. We also used the technique to study time series of convective and stratiform rainfall averaged over 2° by 2° grids in the Amazon basin. The evolution of the precipitation systems, and specifically the transition from convective to stratiform, was well represented by this technique.

We continue our efforts on several aspects of the presented work. Our plan is to compile over a year of collocated IR and MW data to extend the assessment and testing of the technique. Improving the technique's accuracy in predicting convective precipitation is the main goal. This will involve information from additional data sources such as satellite visible and ground-based lightning observations. In a forthcoming separate paper we will demonstrate that the combined use of IR and lightning data can allow a better estimation of the convective rain area and volume.

Acknowledgments: The authors wish to thank Mr. Carlos Morales for assisting them with preliminary processing of the GOES IR data.

References:

Adler, R.F., G.J. Huffman, and P.R. Keehn, 1994: Global tropical rain estimates from microwave-adjusted geosynchronous IR data. *Remote Sensing Reviews*, **11**, 125-152.

Adler, R.F., M.J. Markus, and D.D. Fenn, 1985: Detection of severe midwest thunderstorms using geosynchronous satellite data. *Mon. Weather Rev.*, **113**, 769-781.

Adler, R.F., and A. Negri, 1988: A Satellite Infrared Technique to Estimate Tropical Convective and Stratiform Rainfall. *J. Appl. Meteor.*, **27**, 30-51.

Arkin, P.A., and B.N. Meisner, 1987: The relationship between large-scale convective rainfall and cold cloud over the Western Hemisphere during 1982-1984. *Mon. Wea. Rev.* **115**, 51-74.

Anagnostou, E.N., and C. Kummerow, 1997: Stratiform and Convective Classification of Rainfall Using Satellite 85 Ghz Brightness Temperature Observations. *Journal of Atmospheric and Oceanic Technology*, **14**(3), 570-75.

Atlas, D., D. Rosenfeld, and D.A. Short, 1990: The estimation of convective rainfall by area integrals, Part I: The theoretical and empirical basis. *J. Geophys. Res.*, **95**, 2153-60.

Garreaud, R.D., and J.M. Wallace, 1997: The Diurnal March of Convective Cloudiness over the Americas. *Mon. Weather Rev.*, **125**, 3157-71.

Garstang, M., H.L. Massie, J. Halverson, S. Greco, J. Scala, 1994: Amazon Coastal Squall Lines. Part I: Structure and Kinematics. *Mon. Weather Rev.*, **122**, 608-22.

Greenwald, T.J., G.L. Stephens, T.H. Vonder Haar, and D.L. Jackson, 1993: A physical retrieval of cloud liquid water over the global oceans using special sensor microwave/imager (SSM/I) observations. *J. Geoph. Res.*, **98**, 471-88.

Hartmann, D.L., H.H. Hendon, and R.A. Houze, 1984: Some implications of the mesoscale circulations in tropical cloud clusters for large-scale dynamics and climate. *J. Atmos. Sci.*, **41**, 113-120.

Houze, R.A., 1993: *Cloud Dynamics*. Academic Press.

Houze, R.A., 1997: Stratiform Precipitation in Regions of Convection: A Meteorological Paradox? *Bullet. Amer. Meteor. Soc.*, **78**, 2179-96.

Huffman, G. J. , R. F. Adler, B. Rudolf, U. Schneider, and P. R. Keehn, 1995: A technique for combining satellite-based estimates raingauge analysis, and NWP model precipitation

information into global precipitation estimates. *J. Climate.*, **8(5)**, 1284-1295.

Kummerow, C., W.S. Olson, L. Giglio, 1996: A simplified scheme for obtaining precipitation and vertical hydrometeor profiles from passive microwave sensors. *IEEE Trans. Geosc. & Remot. Sens.*, **34**(5), 1213-32.

Liu, G., J.A. Curry, and R.-S. Sheu, 1995: Classification of clouds over the western equatorial Pacific Ocean using combined infrared and microwave satellite data. *J. Geoph. Res.*, **100**, 811-26, 1995.

Negri, A.J., R.F. Adler, E.J. Nelkin, G.J. Huffman, 1994: Regional rainfall climatologies derived from Special Sensor Microwave Imager (SSM/I) data. *Bull. Amer. Meteor. Soc.*, **75**, 1165-82.

Short, D.A., P.A. Kucera, B.S. Ferrier, J.C. Gerlach, S.A. Rutledge, and O.W. Thiele, 1997: Shipboard Radar Rainfall Patterns within the TOGA COARE IFA. *Bull. Amer. Meteor. Soc.*, **78**, 2817.

Table 1: Data sample statistics

	Calibration site		Validation site	
	Convective	Stratiform	Convective	Stratiform
number of rainy pixels	13,808	49,188	10,492	42,823
Mean (mm/h)	10.81	4.12	10.09	4.23
St. deviation (mm/h)	10.90	4.52	10.60	4.57
coverage (% of total rain volume)	1.3	4.6	0.9	3.6

Table 2: IR algorithm parameter values.

T_{mode} category	< 210 (K)	210-220 (K)	220-230 (K)	230-240 (K)	> 240 (K)
f_T	1.47	0.68	0.42	0.31	0.18
A_{C0}	411	-142	-198	-56	-56
f_C	40,023	11,885	5,828	4,104	1,994

Table 3: Error statistics (CC, FSE, NBIAS) of the IR-derived cloud system rain volumes at the validation site.

Time (LT)		Rain (mm/h)			Area (km^2)		
		CC	FSE (%)	NBIAS (%)	CC	FSE (%)	NBIAS (%)
06	Conv.	.92	71.8	-41.9	.88	76.8	-37.8
	Strat.	.92	66.1	-32.3	.91	66.6	-25.8
	Total	.95	62.6	-35.9	.93	64.3	-28.2
10	Conv.	.84	78.8	-38.8	.84	77.0	-31.0
	Strat.	.91	84.1	-55.2	.91	76.5	-40.4
	Total	.92	76.3	-49.8	.93	71.4	-38.7
18	Conv.	.84	123.8	39.6	.82	108.5	26.8
	Strat.	.87	85.0	31.7	.89	69.3	15.8
	Total	.89	93.7	35.1	.89	70.7	18.3
22	Conv.	.89	70.3	-11.4	.89	65.6	-17.3
	Strat.	.90	66.1	16.1	.91	56.5	6.3
	Total	.93	57.8	4.3	.93	51.0	1.1

Table 4: Conditional error statistics (CC, upper rows; FSE (%), middle rows; and NBIAS (%), lower rows) of instantaneous area-averaged rainrates derived from the IR technique over the selected 2° by 2° grids.

Local time	Site 1	Site 2	Site 3	Site 4
06	0.93 58.1 -3.9	--	0.43 175.2 -61.8	--
10	0.85 88.9 -45.2	0.78 99.4 -51.1	--	0.62 112.1 -69.3
18	0.83 107.7 38.7	0.97 34.6 26.9	0.89 113.6 56.5	0.82 81.0 11.1
22	0.85 77.4 15.3	0.98 29.8 -12.6	0.86 71.8 6.6	0.62 105.0 -18.5

Table 5: Same as in Table 4, but the instantaneous area-averaged rainrates are derived from the single IR-rainrate relationship.

Local time	Site 1	Site 2	Site 3	Site 4
06	0.84 94.0 -4.5	--	0.41 184.7 -50.1	--
10	0.65 149.7 -77.2	0.76 127.2 -73.4	--	0.73 137.7 -98.6
18	0.83 132.2 63.0	0.98 101.4 87.6	0.89 160.8 85.0	0.85 104.9 44.1
22	0.89 65.5 -15.8	0.95 50.4 -37.9	0.82 80.9 -13.0	0.58 113.1 -34.5

Figures caption

Figure 1: Histograms of convective and stratiform rain rates derived from microwave data at 12.5 Km resolution.

Figure 2: Study area, showing the calibration and validation sites, as well as four representative areas examined in greater detail.

Figure 3: Scatter plots of cloud system area (A_{mode}) versus microwave-derived rain area for six classes of mode IR temperature (T_{mode}).

Figure 4: Scatter plots of convective index versus cloud system's convective area for four T_{mode} classes.

Figure 5: Upper panel: Cloud-top IR temperatures (shaded, gray scale in degrees Kelvin), T_{mode} isotherm (blue contours), and local minima locations (red crosses). Middle panel: IR technique-derived convective (red) and stratiform (blue) areas. Lower panel: MW-based convective-stratiform areas. The domain size (10° by 15°), and resolution (12.5 km) are the same as for all the panels.

Figure 6: IR temperature depression from 253K versus MW-derived convective (solid lines) and stratiform (dashed lines) rain rate at 12.5 km resolution; presented for four T_{mode} classes.

Figure 7: Examples of IR technique-derived (upper panels) and MW(GPROF) (lower panels) instantaneous rain rate fields. The domain size (15° by 10°), resolution (12.5 km), and color scale (four levels: 0-5, 5-10, 10-20, >20 mm/h) are the same as for all the panels.

Figure 8: Scatter plots of IR technique-derived versus MW-based convective and stratiform areas (km^2).

Figure 9: Scatter plots of IR technique-derived versus MW-based convective and stratiform rain volumes (mm km^2).

Figure 10: IR versus MW-based unconditional mean convective and stratiform rainfall over four 2° grid areas in the Amazon.

Figure 11: IR temperature versus MW-derived rain rate at 12.5 km resolution based on the area-matching method.

Figure 12: Mean monthly rainfall (mm/month) for the period January-April (1996) presented at hourly time ranges (0-1, 1-2, [...], 22-23, and 23-24 GMT reading from left to right and top to bottom).

Figure 13: Histograms of convective and stratiform rain rates derived from the IR technique at 12.5 Km resolution.

Figure 14: IR technique-derived diurnal variations of average convective rainfall rate (solid lines), and stratiform rainfall rate (dashed lines) for the selected 2° grid areas in the Amazon.

Figure 15: Time series of area-averaged convective and stratiform rainfall derived from the IR technique.

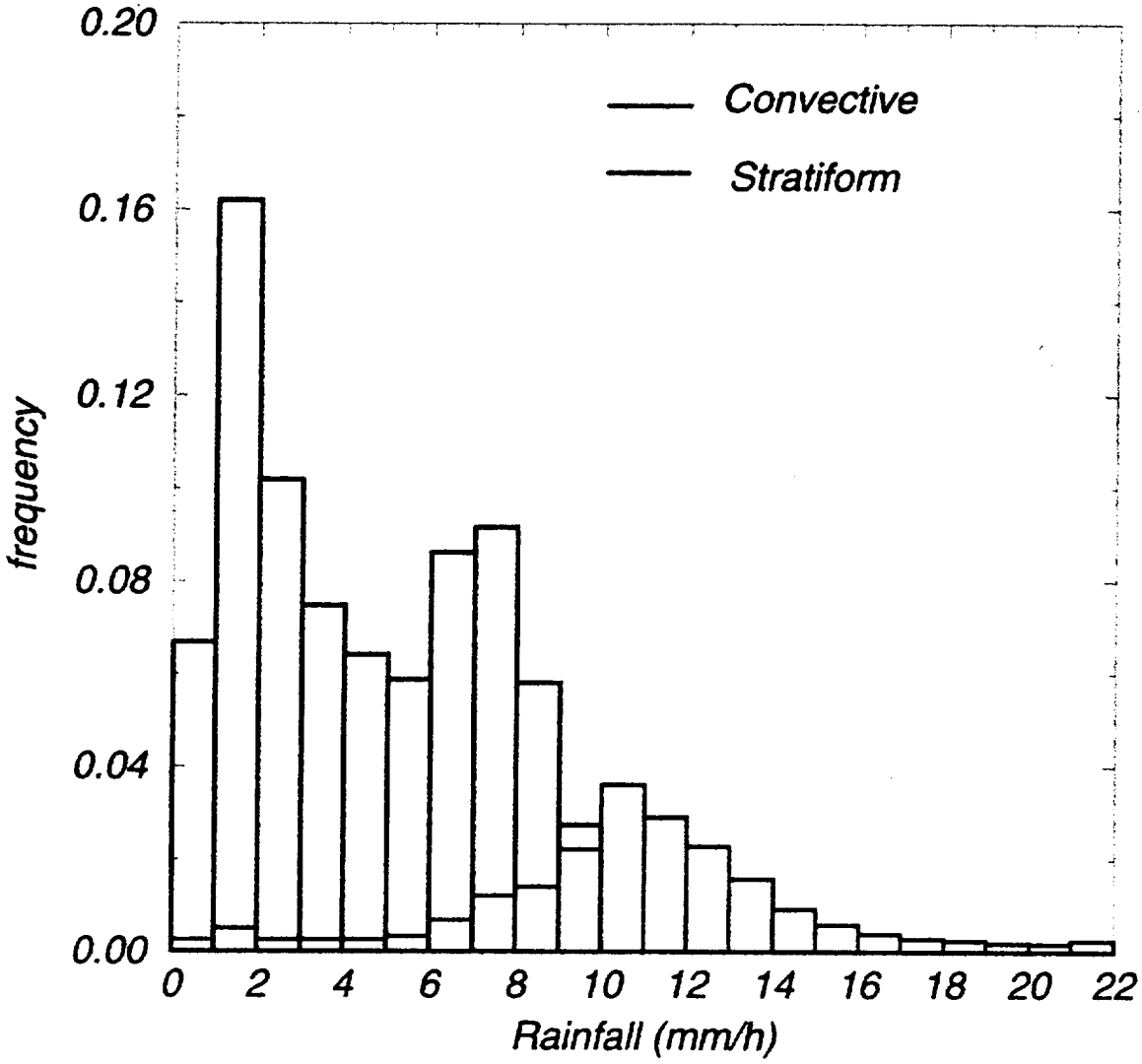
0.20
0.16
0.12
0.08
0.04
0.00
frequency
Convective
Stratiform
0
2
4
6
8
10
12
14
16
18
20
22
Rainfall (mm/h)

(1)

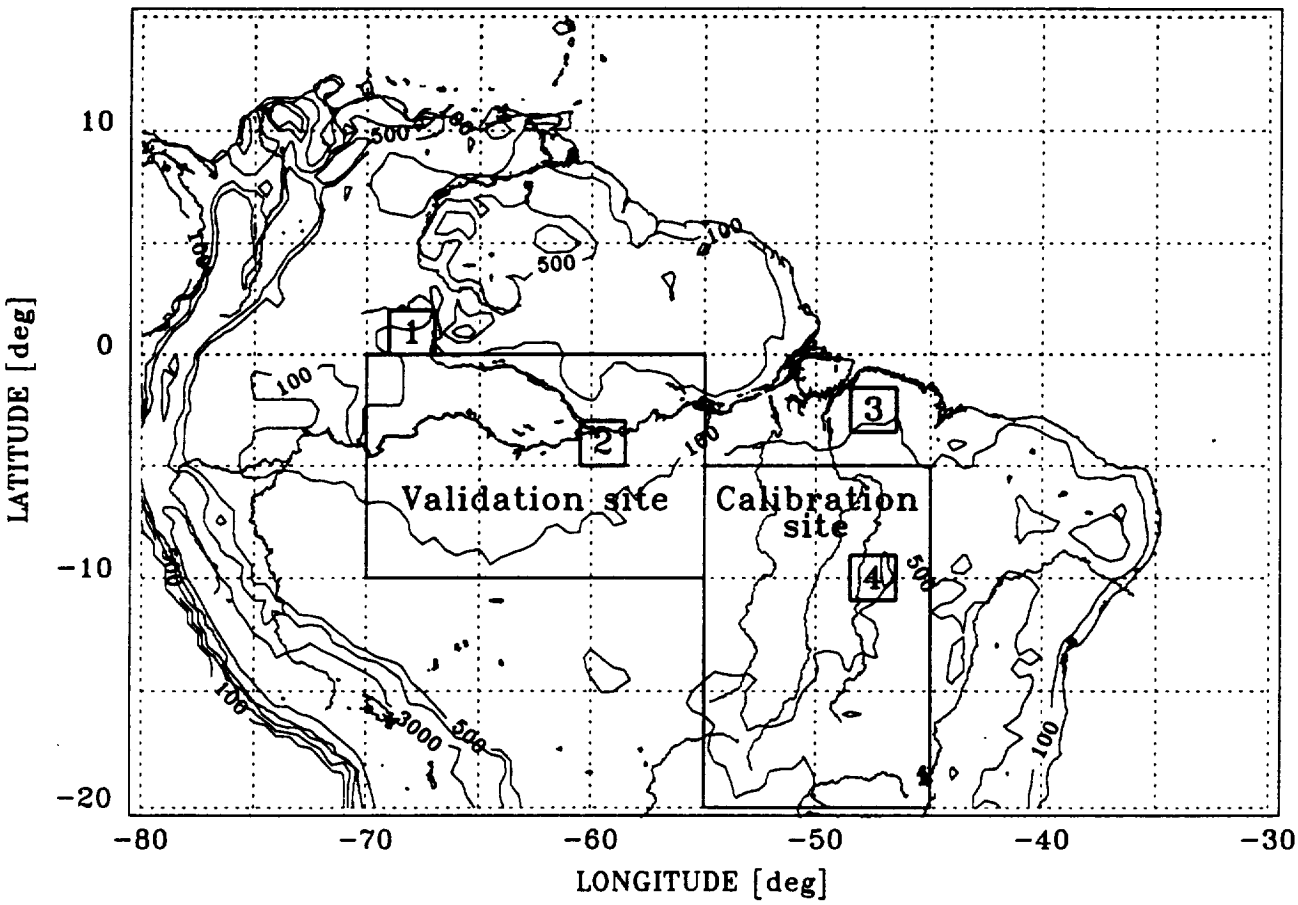
10
0
−10
−20
LATITUDE [deg]
−80
−70
−60
−50
−40
−30
LONGITUDE [deg]
1
2
3
4
Validation site
Calibration site
100
500
3000

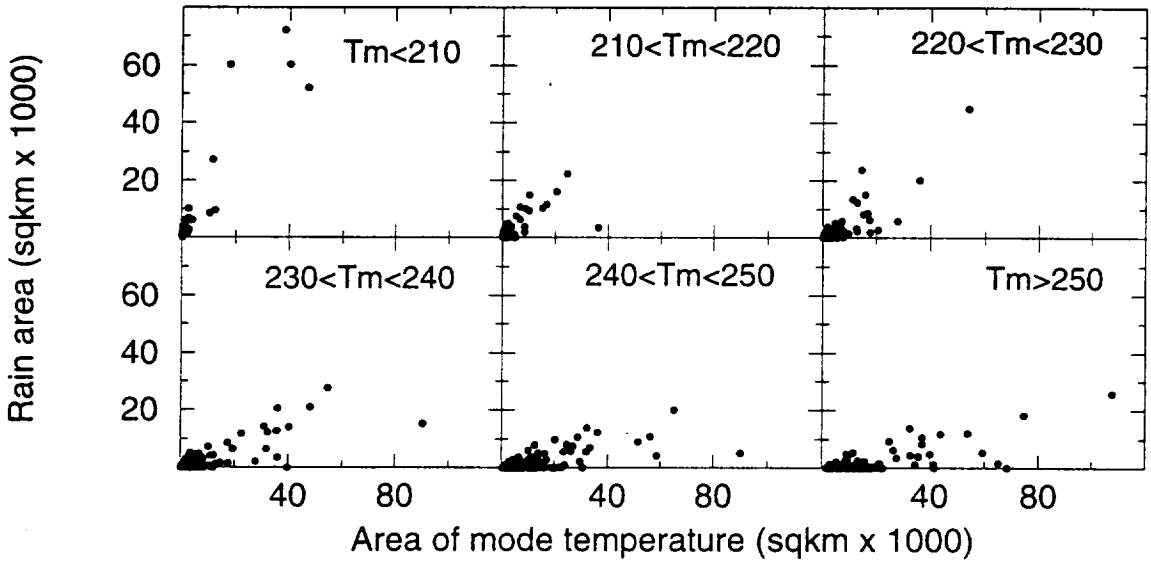
Tm<210
210<Tm<220
220<Tm<230
230<Tm<240
240<Tm<250
Tm>250
Rain area (sqkm x 1000)
60
40
20
40
80
Area of mode temperature (sqkm x 1000)

(3)

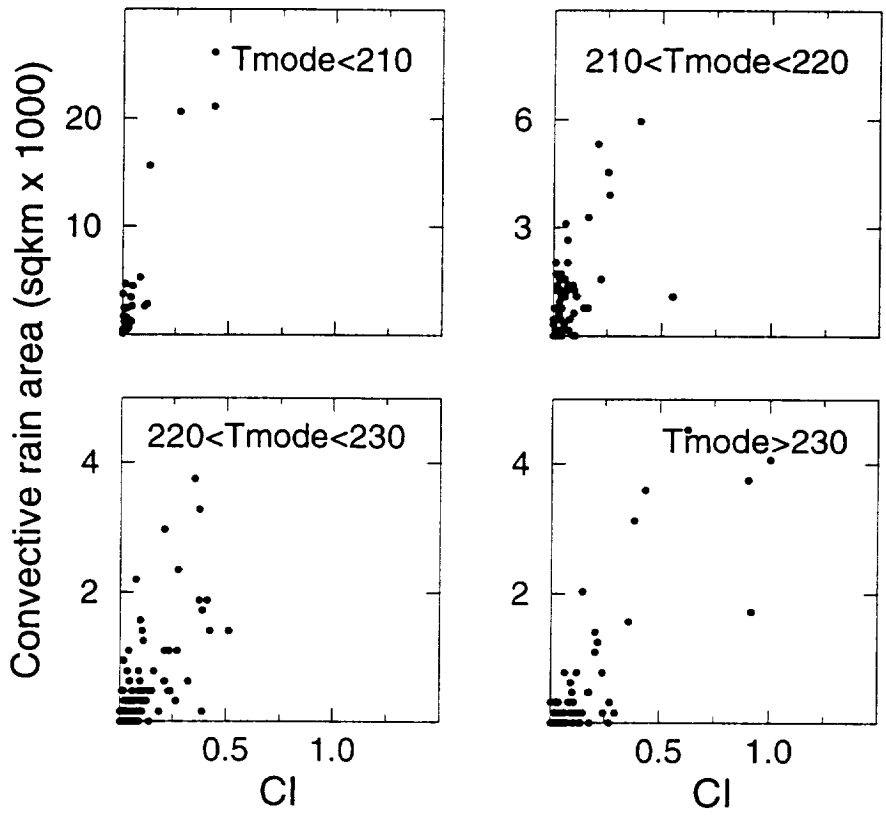
Tmode<210
210<Tmode<220
220<Tmode<230
Tmode>230
Convective rain area (sqkm x 1000)
20
10
6
3
4
2
4
2
0.5
1.0
0.5
1.0
CI
CI

(4)

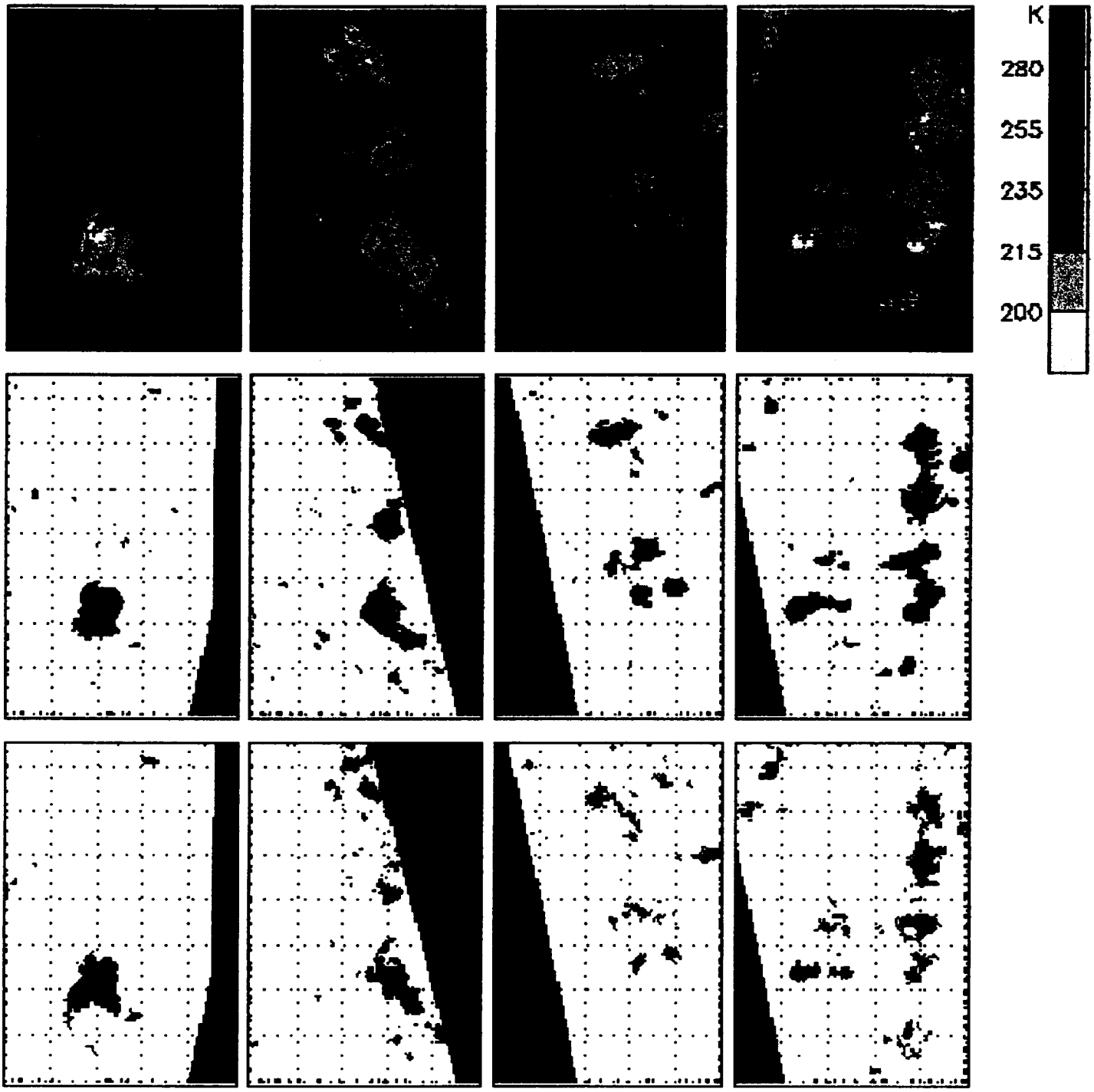

(5)

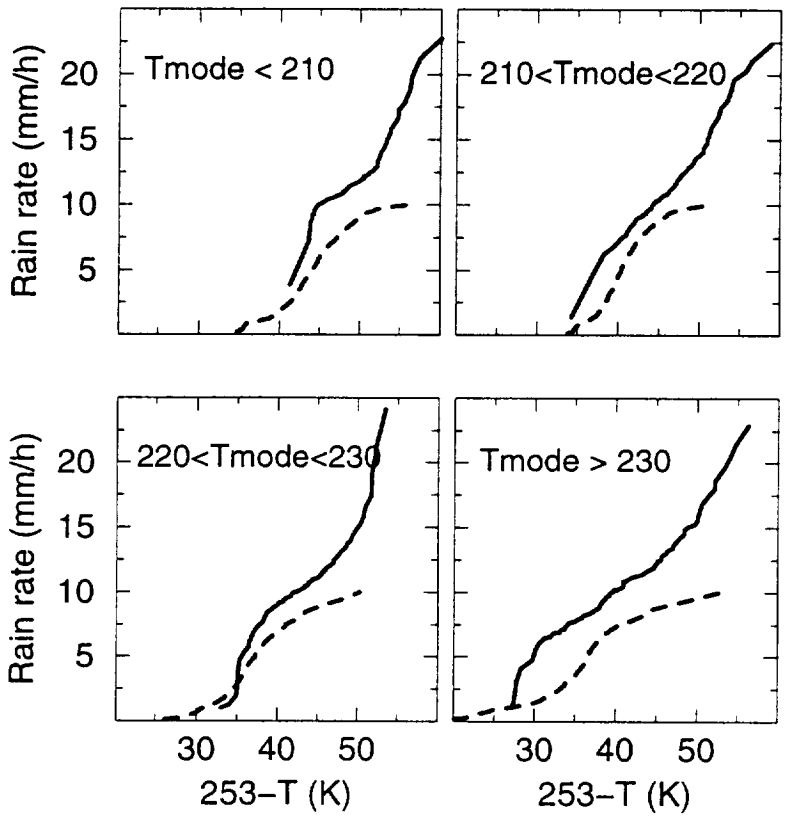
Tmode < 210
210<Tmode<220
220<Tmode<230
Tmode > 230
Rain rate (mm/h)
Rain rate (mm/h)
20
15
10
5
20
15
10
5
30
40
50
30
40
50
253–T (K)
253–T (K)

IR

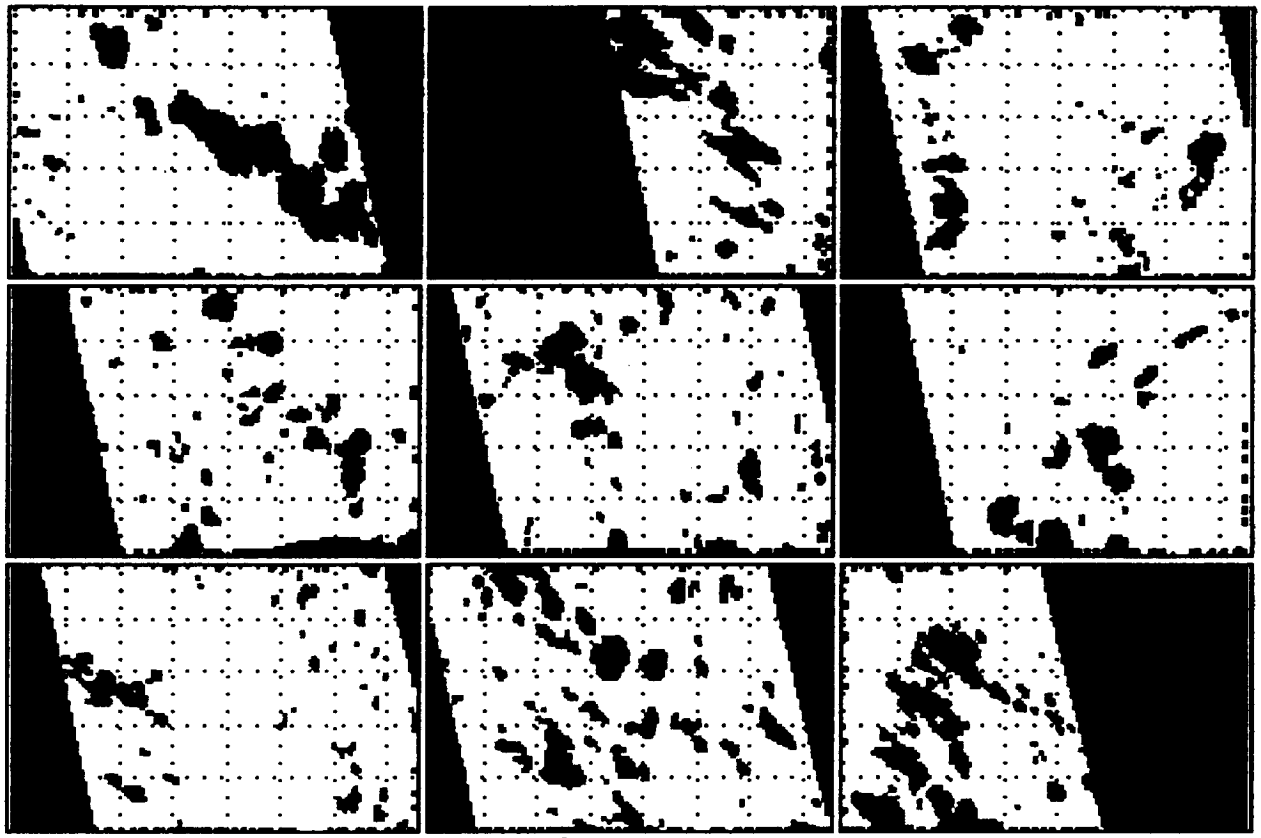

Microwave

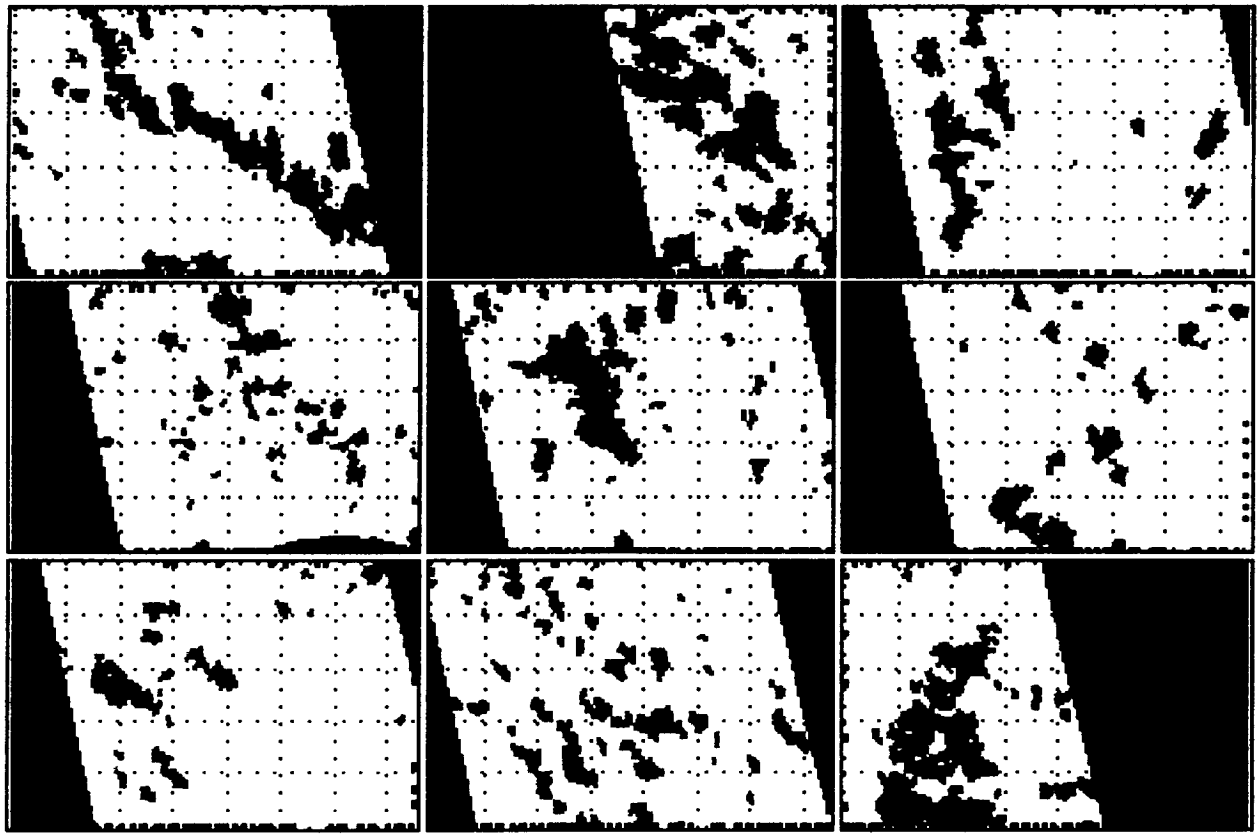

(7)

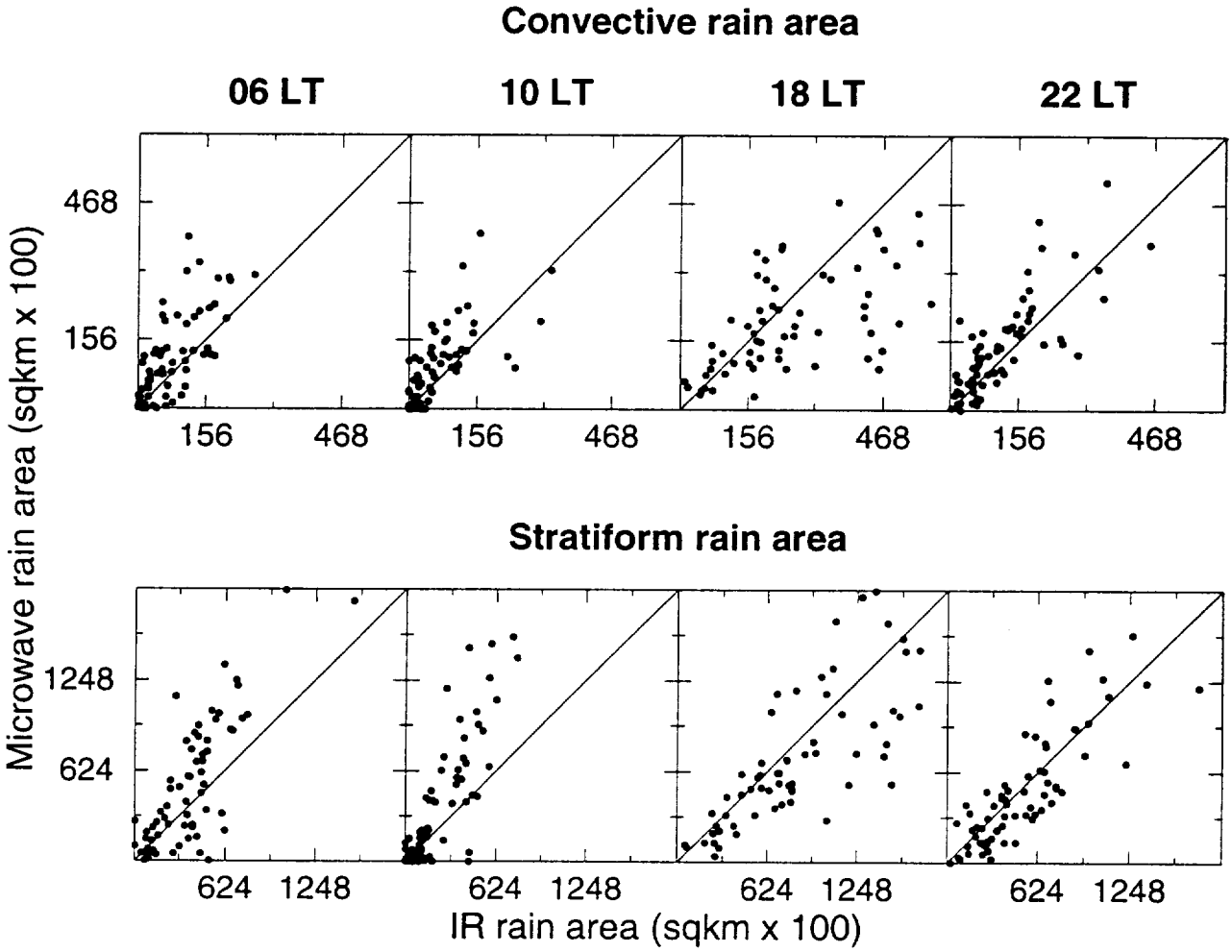
Convective rain area
06 LT
10 LT
18 LT
22 LT
468
156
156
468
Stratiform rain area
1248
624
624
1248
Microwave rain area (sqkm x 100)
IR rain area (sqkm x 100)

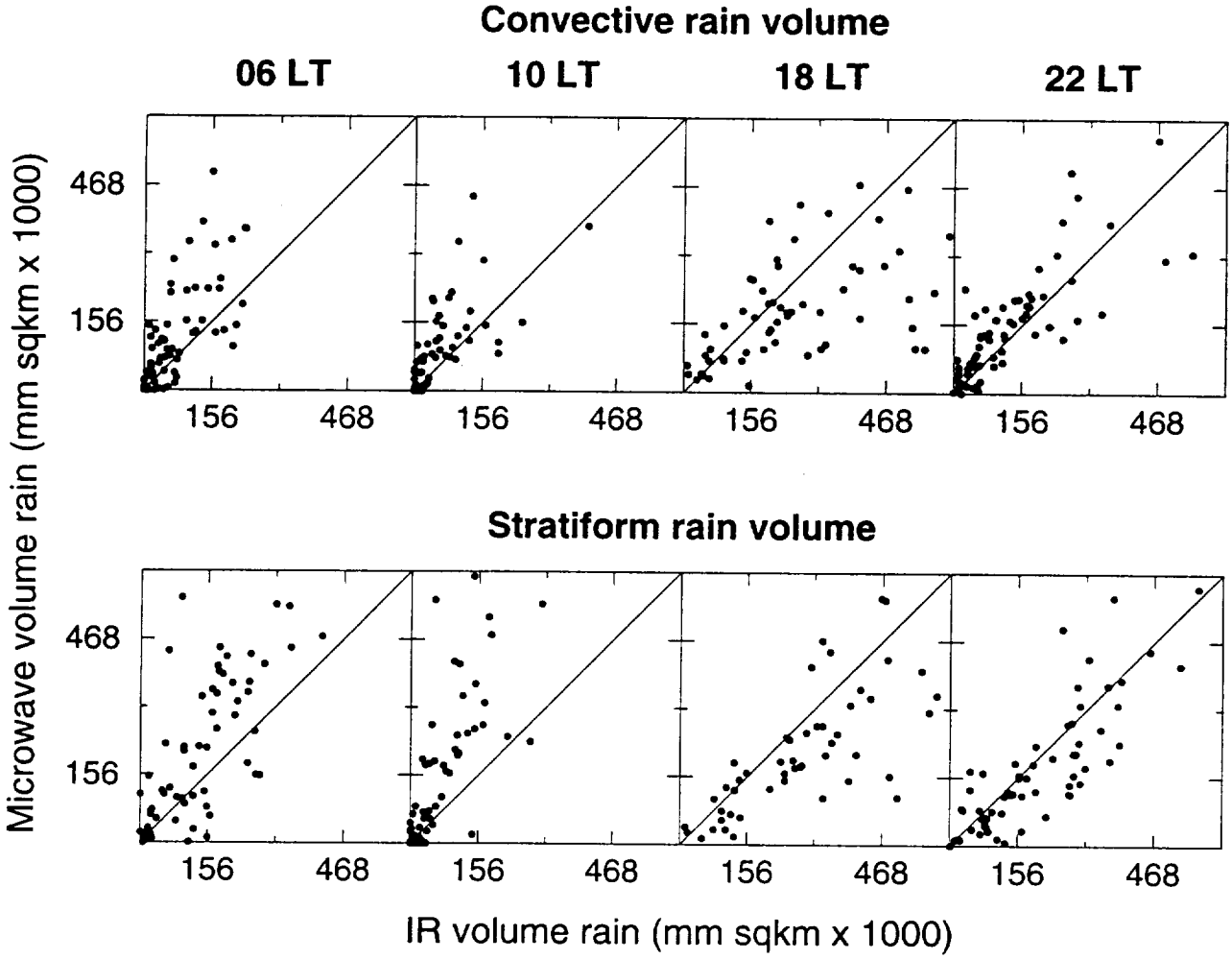
Convective rain volume
06 LT
10 LT
18 LT
22 LT
468
156
156
468
Stratiform rain volume
Microwave volume rain (mm sqkm x 1000)
IR volume rain (mm sqkm x 1000)

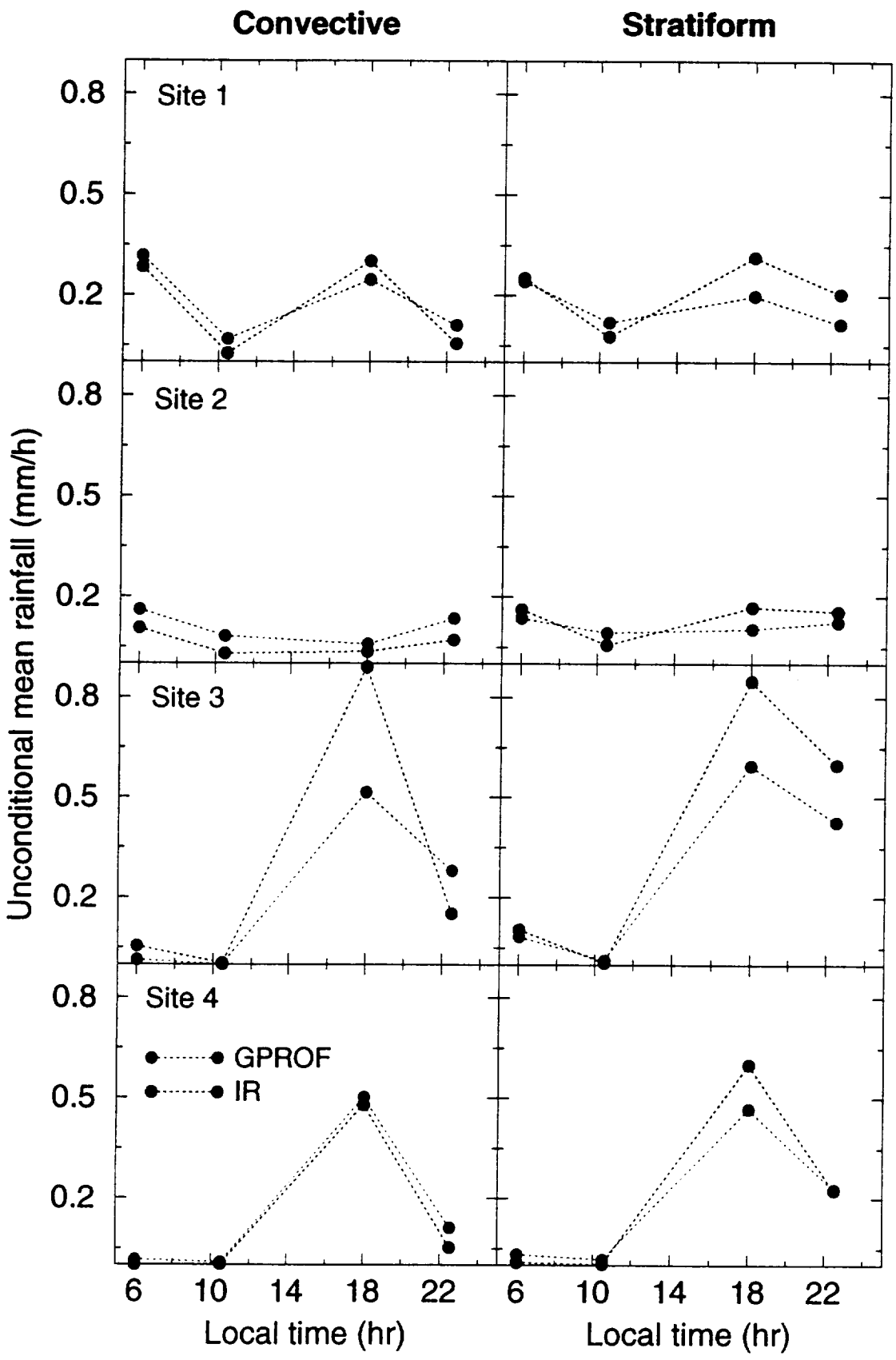
Convective
Stratiform
Site 1
Site 2
Site 3
Site 4
GPROF
IR
0.8
0.5
0.2
Unconditional mean rainfall (mm/h)
6
10
14
18
22
Local time (hr)

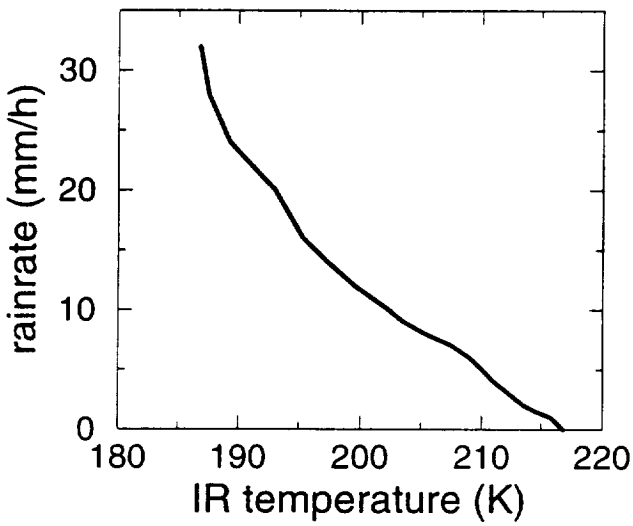

(11)

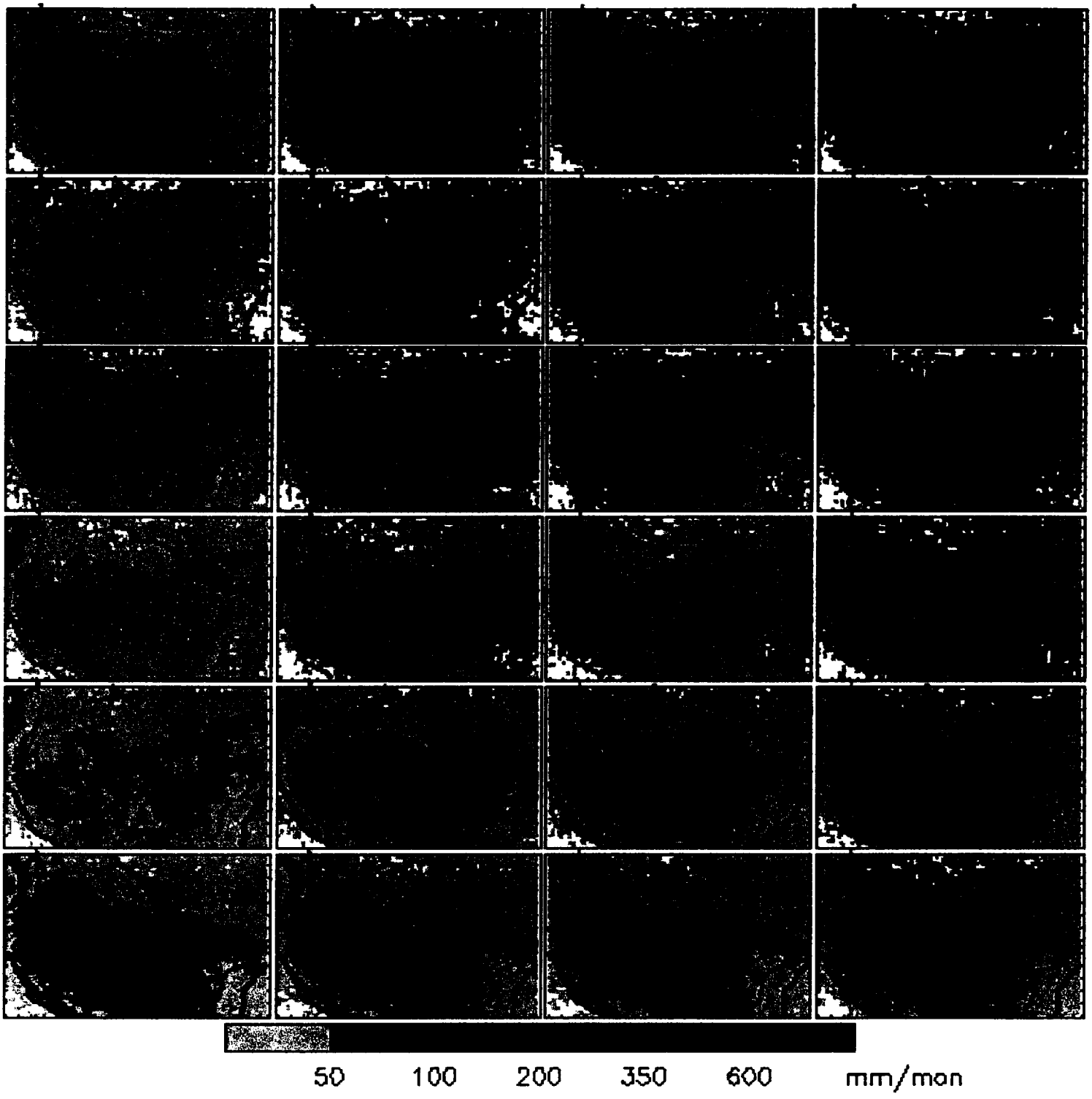
50
100
200
350
600
mm/mon

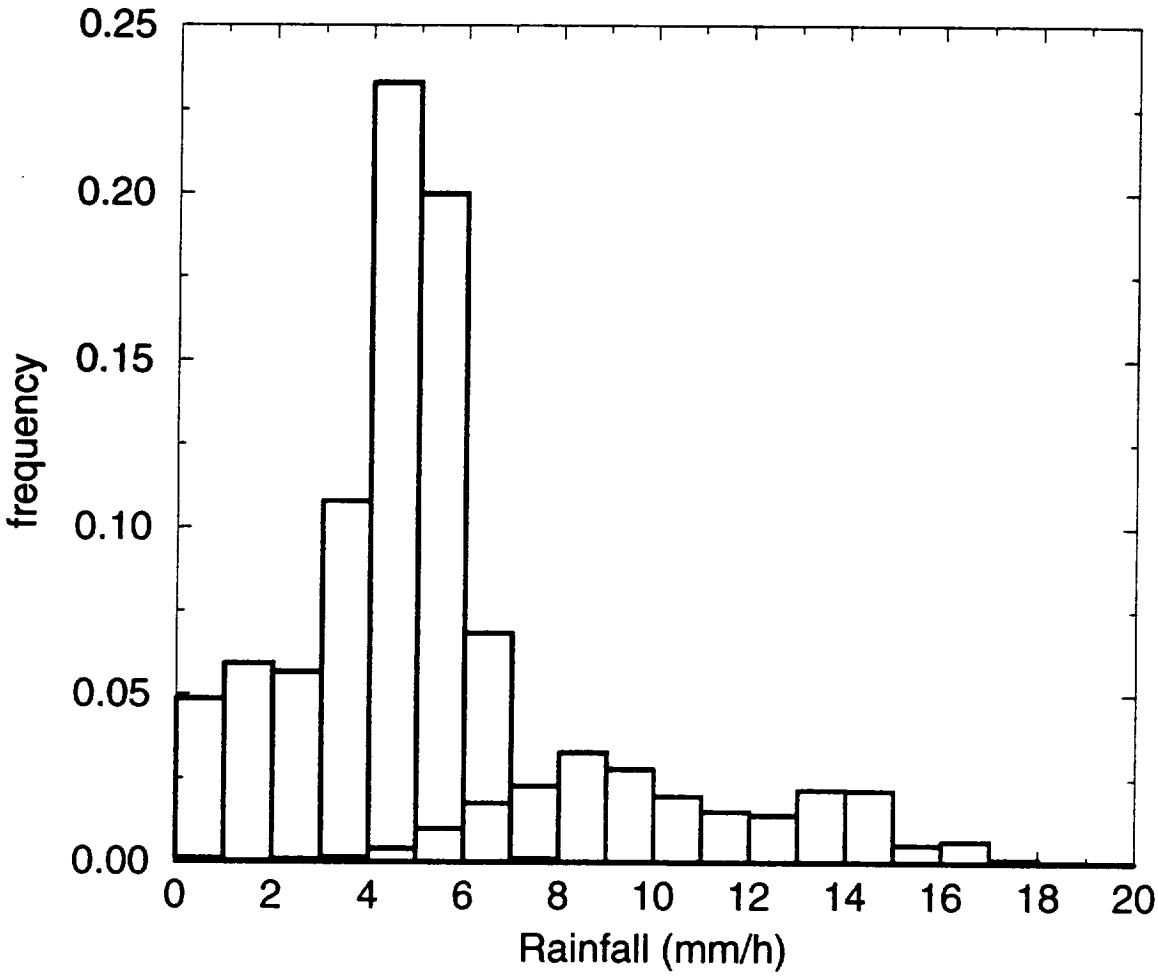
0.25
0.20
0.15
0.10
0.05
0.00
frequency
0
2
4
6
8
10
12
14
16
18
20
Rainfall (mm/h)

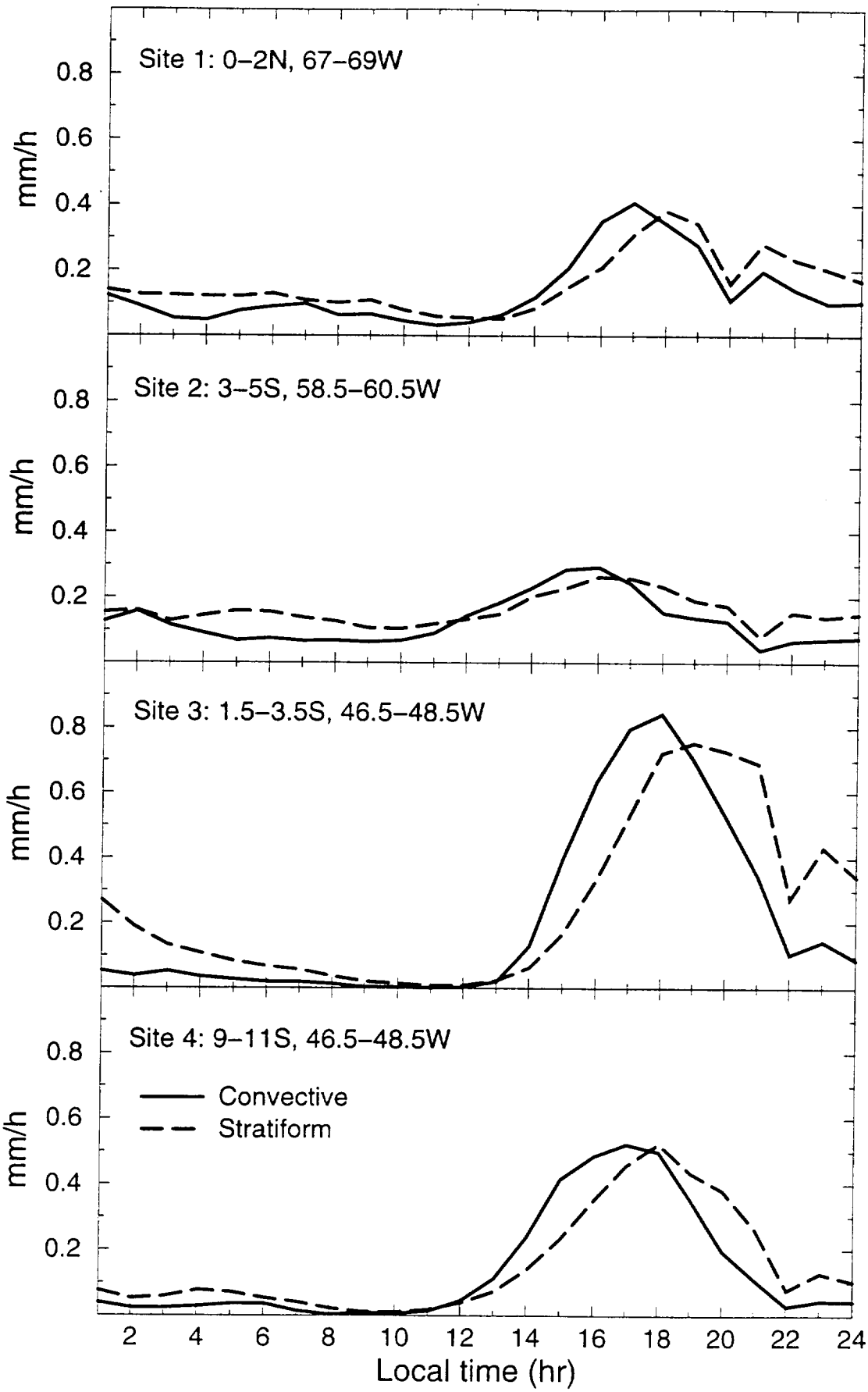
Site 1: 0–2N, 67–69W
Site 2: 3–5S, 58.5–60.5W
Site 3: 1.5–3.5S, 46.5–48.5W
Site 4: 9–11S, 46.5–48.5W
Convective
Stratiform
mm/h
0.8
0.6
0.4
0.2
2
4
6
8
10
12
14
16
18
20
22
24
Local time (hr)

(12)

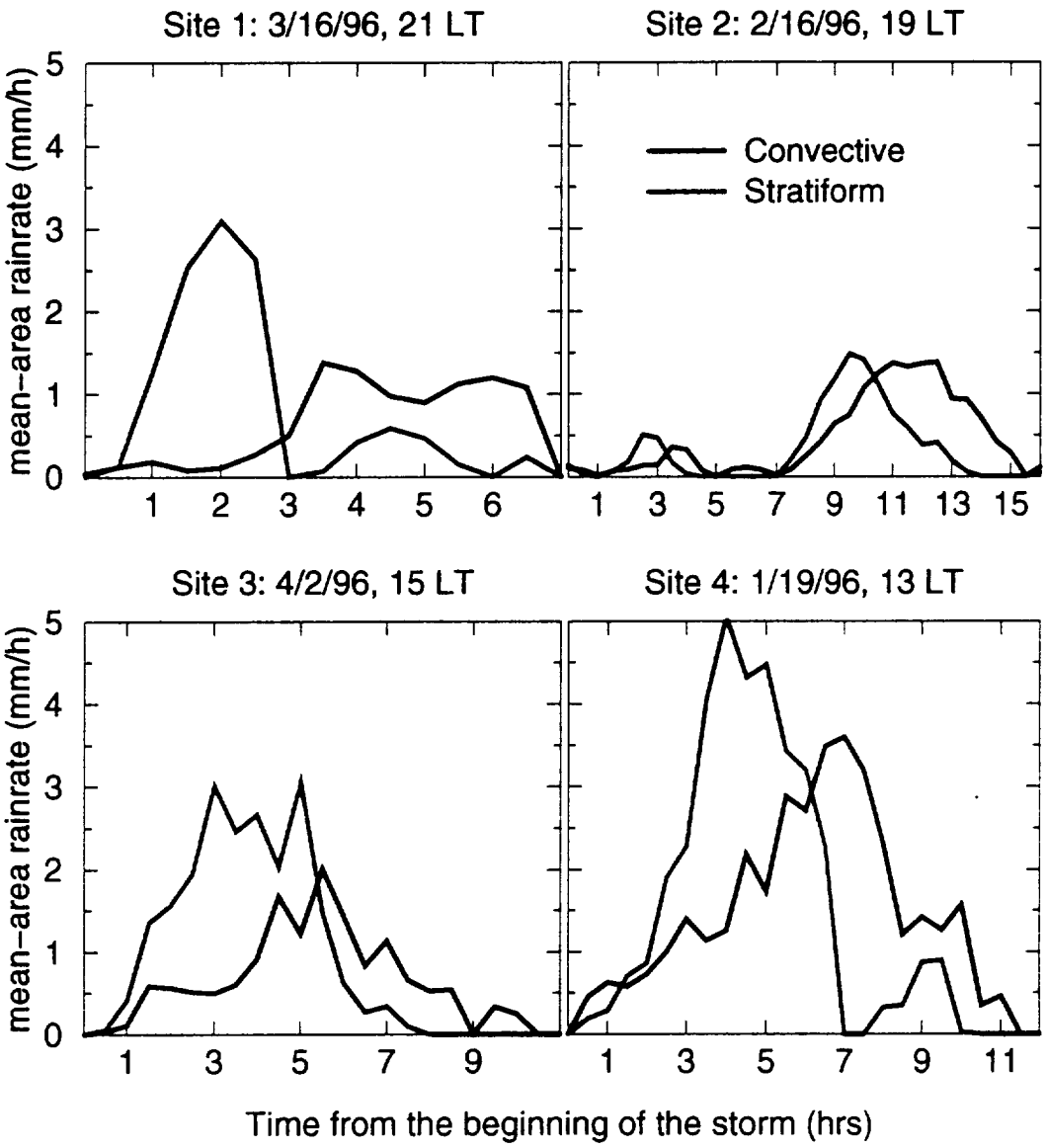
Site 1: 3/16/96, 21 LT
Site 2: 2/16/96, 19 LT
Site 3: 4/2/96, 15 LT
Site 4: 1/19/96, 13 LT
Convective
Stratiform
mean-area rainrate (mm/h)
Time from the beginning of the storm (hrs)